# Particle Response to Shock Waves in Solids: Dynamic Witness Plate/PIV Method for Detonations

**Michael J. Murphy [1], Ronald J. Adrian[1]**

1: Department of Mechanical and Aerospace Engineering, Arizona State University, Tempe, USA,
mjmurphy1@asu.edu, rjadrian@asu.edu

**Abstract** Studies using transparent, polymeric witness plates consisting of polydimethlysiloxane (PDMS) have been conducted to measure the output of exploding bridge wire (EBW) detonators and exploding foil initiators (EFI). Polymeric witness plates are utilized to alleviate particle response issues that arise in gaseous flow fields containing shock waves and to allow measurements of shock-induced material velocities to be made using particle image velocimetry (PIV). Quantitative comparisons of velocity profiles across the shock waves in air and in PDMS are made to demonstrate the improved response achieved by the dynamic witness plate method. Schlieren photographs are used to complement analysis through direct visualization of detonator-induced shock waves in the witness plates.

## 1. Introduction

To achieve PIV measurements in blast waves resulting from micro-detonations it is essential for the particle markers to follow the extreme accelerations characteristic of shocks. A new method to study this type of flow has been proposed by Murphy et al. (2005). In this method detonator output is characterized by placing a transparent polymeric witness plate adjacent to the detonation and observing the shock-induced velocity field within the witness plate by pulsed schlieren imaging and particle image velocimetry (PIV). In principle, the high density of the polymer, relative to that of the gas, makes the particles much more responsive to accelerations, thereby making the PIV measurements more accurate.

Using an approximate expression for particle slip velocity at finite Reynolds number (Adrian 1991) given as

$$\left|\mathbf{v}_\mathrm{p}-\mathbf{u}\right|=\left(\frac{2}{3}\frac{\rho_\mathrm{p}}{\rho}\frac{d_\mathrm{p}}{C_\mathrm{D}}\left|\frac{\mathrm{d}\mathbf{v}_\mathrm{p}}{\mathrm{d}t}\right|\right)^{1/2}, \qquad (1)$$

the lag velocity is shown to be proportional to the square root of the ratio of particle density to fluid density, $(\rho_p/\rho)^{1/2}$. For the typical case of liquid particles in air, the quantity $(\rho_p/\rho)^{1/2}$ is approximately 30. By replacing the gas with a solid having seed particles embedded in it, the slip velocity can be reduced by roughly 30:1, since $(\rho_p/\rho)^{1/2}$ is now approximately unity.

By demonstrating feasibility, the witness plate/PIV method has only been introduced as a viable means of obtaining quantitative data of micro-detonator output, like the exploding bridge wire (Murphy et al. 2005). Current efforts focus on introducing the effectiveness of the method by demonstrating significant improvement in particle response in regions containing detonator-induced shocks. This is accomplished by making quantitative comparisons of velocity profiles across the shock waves in air and in the witness plates. The profiles are obtained from vector fields of shock-induced material velocities in the polymer.

In this work it will be shown that the dissimilar outputs of two types of micro-detonators can be characterized and compared using the witness plate/PIV method complemented by schlieren photography employing laser backlighting.

# 2. Experiment

## 2.1 Impact detonators

The present work focuses on two types of impact detonators, model SE-1 exploding bridge wires (EBW) and exploding foil initiators (EFI) utilizing flyer plates. The latter device is also known as a slapper detonator and will be referred to as such hereafter. Both detonator types are manufactured and provided by Los Alamos National Laboratory (LANL), and each device utilizes a metal bridge that is exploded by quickly discharging electrical current across the bridge in durations of approximately one microsecond. For the case of the EBW the metal wire is gold, and the shock resulting from the wire explosion is used to directly shock-initiate an explosive through surface impact. A slapper detonator functions in a different manner but still results in impact initiation of an explosive.

An entire slapper detonator typically consists of a dielectric base plate, a bridge that is chemically etched onto a metal foil, a thin dielectric sheet attached to the top surface of the metal foil, and a barrel placed directly above the bridge location. Upon explosion of the metal bridge, the explosive forces cause a piece of the dielectric sheet in between the bridge and the bottom end of the barrel to shear off and accelerate through the barrel. The resulting dielectric flyer plate emerges from the top end of the barrel at supersonic speed and impacts an explosive pellet by delivering a short-duration shock pulse (Cooper and Kurowski, 1996). The slapper device in this work contains a copper bridge and a polyimide flyer plate. A photograph of the metal bridge of each detonator is shown in Fig. 1 along with typical bridge dimensions.

Notice the direct output of each detonator is not similar. The EBW produces a shock wave and the slapper produces a flyer plate. The drastic differences between the outputs of each detonator necessitate the use of a witness plate to make comparisons of detonator impact characteristics, such as the strength of the shock induced from impact. Consequently, particle-seeded polymers are utilized so that measurements of shock-induced material velocities can be made using PIV, where the shocks result from the impact mechanism of each detonator.

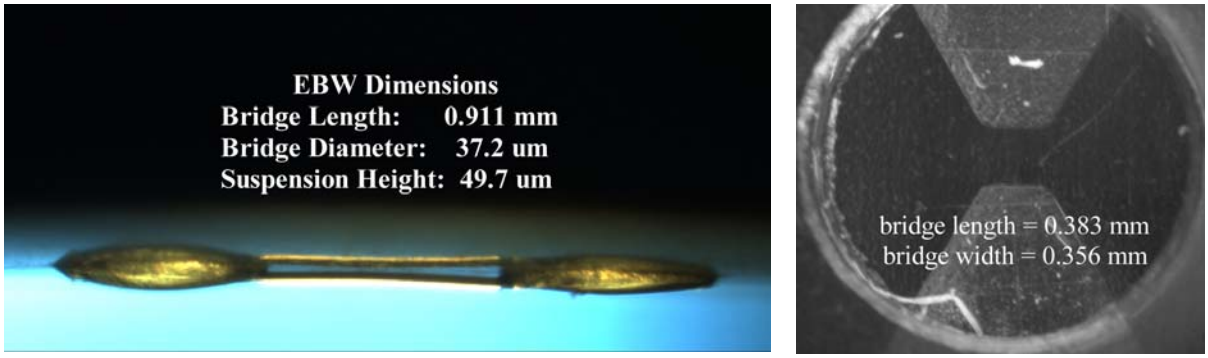


Fig. 1. Photograph of gold EBW and copper EFI

## 2.2 Witness plates

The silicone polymer polydimethlysiloxane (PDMS) is utilized for these experiments and is made and distributed by Dow Corning as Sylgard 184. The longitudinal wave speed is acoustically measured as 1.04 mm/μs +/- 1% using a standard pulse-echo measuring technique (Cartz 1995). The polymer density is 1.03 g/cm$^3$ and the index of refraction is provided by Dow Corning as 1.41. Since the PDMS samples must be cured as a mixture of a curing agent with water-like viscosity and a pre-polymer with honey-like viscosity, the desired concentration of seed particles is thoroughly mixed into the curing agent prior to combining it with the pre-polymer. This is done to ensure the particles are uniformly distributed and do not agglomerate. The resulting particle mixture is combined with the pre-polymer and depressurized in a vacuum chamber to eliminate any bubbles in

the sample. Molds are constructed from glass microscope slides since they have smooth surfaces and convenient dimensions, and the final PDMS mixture is carefully poured into the molds. The samples are placed on a hot plate for approximately four hours to cure, after which the glass molds are removed and the particle-seeded PDMS witness plates are ready to use.

PDMS samples having dimensions of 25 mm (L) x 25 mm (W) x 13 mm (H) are seeded with metallic-coated glass micro-spheres that have a density of 2.6 g/cm$^3$ (TSI, Inc.). The spheres have a nominal mean diameter of 9 μm, but range in actual size from 4 to 16 μm. The particle concentration is chosen such that 3-5 particles lie within a field of view of 100 μm (L) x 100 μm (W), which corresponds to a minimum interrogation window size of approximately 16 pixels (L) x 16 pixels (W). Even when seeded with a large concentration of particles, the resulting PDMS samples maintain a high degree of transparency.

## 2.3 Experimental PIV setup

A schematic of the particle-illumination system is shown in Fig. 2. A pair of New Wave Research 120 mJ, pulsed Nd:YAG lasers are utilized for particle illumination. The nominal pulse width of each laser is 5 ns, and the minimum laser sheet thickness is measured as 260 μm. The imaging objective lens is a 105 mm Nikon lens (AF Micro-Nikkor) operated at $f$/5.6 with a maximum magnification of 1:1. The resulting field of view is approximately 4 mm (W) by 4 mm (H).

Experimental PIV images are recorded using the Imacon 200 ultra-fast CCD camera described in Murphy and Adrian (2005). The camera design is well suited for making PIV measurements since the CCD arrays operate in an effective frame-straddle mode. The biggest advantage of using this particular camera for PIV is the improvement in temporal resolution over standard commercial PIV cameras utilizing interline data-transfer technology.

A typical commercial PIV camera operating at a frame rate of 30 Hz in dual-exposure mode can allow two exposures to be obtained with a minimum inter-frame delay time of roughly 200 ns. The length of the first exposure is commonly around 250 μs, but the second exposure remains sensitive to light for nearly 33 ms due to the maximum frame rate of the camera. Consequently, any background radiance present in the field of view will saturate the CCD array over the lengthy extent of the second exposure. This effect has been successfully reduced by employing a liquid-crystal variable attenuator as an optical shutter (Balakumar and Adrian, 2004), but in the work presented here this type of solution is inadequate in reducing the inherent background luminance resulting from detonator blasts.

Unlike commercial PIV cameras, the Imacon 200 camera design permits each exposure to be reduced to as small as 5 ns with 5 ns inter-frame delays.

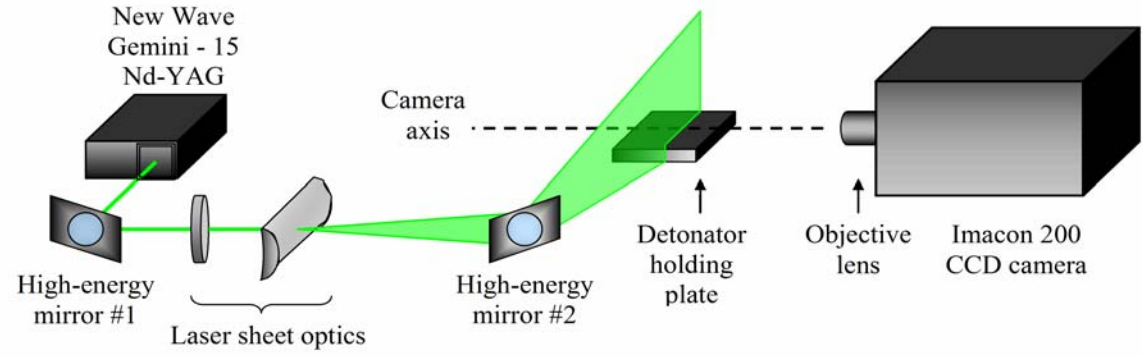


Fig. 2. Diagram of experimental PIV setup

## 2.4 Temporal synchronization

Experimental timing parameters for the PIV system utilizing the Imacon camera are manually controlled using two digital delay/pulse generators, a Stanford Research Systems (SRS) DG 535 and a Berkeley Nucleonics Corporation (BNC) model 555. A 10 Hz positive TTL pulse from channel AB of the SRS unit is continuously sent into the external trigger of the laser flash lamps causing them to repeatedly fire every 100 ms. This maintains a consistent population inversion within the laser cavities that is important for ensuring consistent output pulse energy each time the Q-switches are triggered. The same trigger pulse from the SRS unit is directed into the external trigger input of the BNC box via the $T_0$ output channel. A delay sequence programmed into channels A, B, C, and D governs the operation of the camera, laser Q-switches, and capacitor-discharge unit used to initiate each detonator. Once the BNC box is triggered the timing sequence of all channels is activated exactly once. Delay specifics for each channel, as well as a timing diagram of the experimental delay sequence, are shown in Fig. 3. Values of $t_0$, $t_b$, $t_{event}$, and $\Delta t$ are obtained from voltage traces from a current-viewing resistor in the CDU circuit.

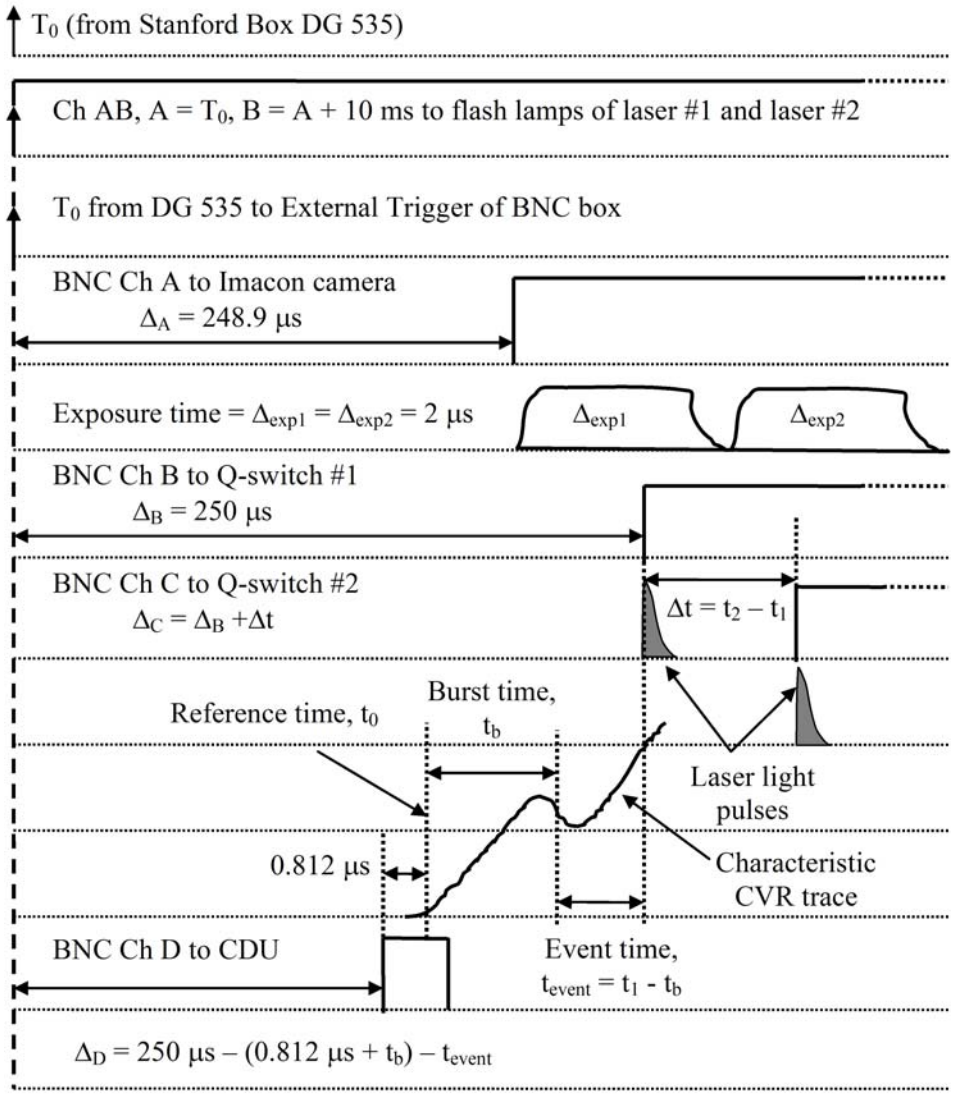


Fig. 3. Timing diagram for witness plate/PIV experiments

## 2.5 Experimental schlieren setup

Two types of schlieren configurations are used for these experiments. The first is a standard z-type configuration using front-surface, parabolic mirrors and a pulsed, argon light source. This setup is described in Murphy et al. (2005) and will not be repeated here. The second system is an in-line, lens-type system depicted in Fig. 4.

Light from a Coherent 500 mW, continuous Nd:YAG laser (DPSS 532) is passed through a spatial filter and used as an intense extended source for backlighting. With the position of the light source fixed at the location of the spatial filter, a positive lens (L1) is used as an effective light collimator by carefully positioning it such that its focal point coincides with the location of the source. The resulting collimated light then passes through the experimental region of interest and is used to align the camera axis precisely parallel to that of the incident light. A second positive lens (L2) is carefully placed between the region of interest and the camera in order to focus the light to a point, prior to entering the camera. A standard razor blade functions as the knife edge at the point of focus of L2. A 105 mm Nikon objective lens (AF Micro-Nikkor) is utilized on the camera to image the object plane onto the image plane, which is defined by the location of the CCD array in the camera.

The immediate benefit of using a laser backlight is that the intense light emission from the detonator blasts can be attenuated prior to entering the camera by employing a small-bandwidth bandpass filter (Andover). Use of the filter allows visualizations to be obtained of the first 1-2 μs of a detonator blast, when the intensity of the explosive flash is at a maximum. A continuous backlight is permissible due to the ultra-fast shuttering capability of the Imacon camera. Small exposure widths of 200 ns are used to effectively freeze the motion of the shock waves in PDMS.

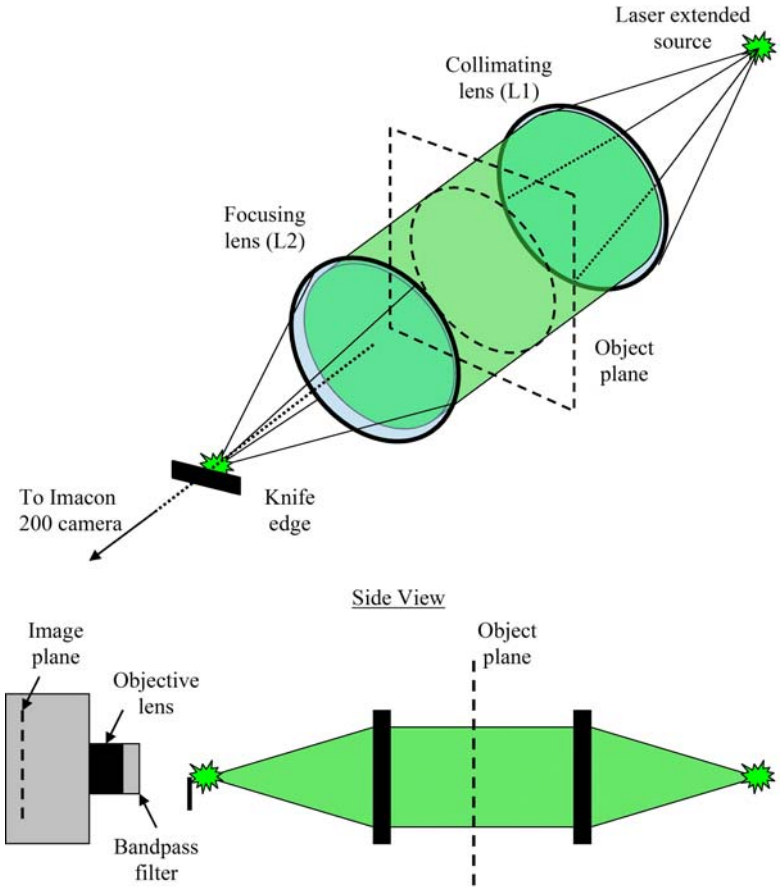


Fig. 4. Diagram of in-line schlieren setup

# 3. Results and Discussion

## 3.1 Schlieren visualization of shocks

The direct yield from an EBW and slapper detonator is visualized propagating into ambient air using schlieren photography, and the results are displayed in Fig. 5a and 5b, respectively. The corresponding impact-induced shock-fronts in PDMS are also visualized and displayed in Fig. 5c and 5d. For detonator initiation in air a moderate input charge voltage of 1 kV is used in order to reduce the intensity of emitted light from the bridge explosion. This ensures the yield characteristics of each detonator can be easily investigated in the absence of intense explosive flash.

Notice the induced-shocks in PDMS appear to grow radially in space for each detonator operated with an initial charge voltage of 3.02 kV. This observation is expected since on the scale of a few millimeters both the EBW and flyer plate effectively impact the witness plate surface as a point source. The visualizations obtained from flyer-plate impact display additional peripheral shocks spanning outward from the central disturbance. The cause of such shocks has not been completely determined though we postulate edge effects from the impacting flyer plate may be the cause. Nonetheless, evidence of shock fronts propagating approximately radially through PDMS due to initiation of EBW and slapper detonators is successfully obtained using schlieren photography. The visualizations provide insight into the expected flow geometry that should be displayed in the ensuing PIV investigations.

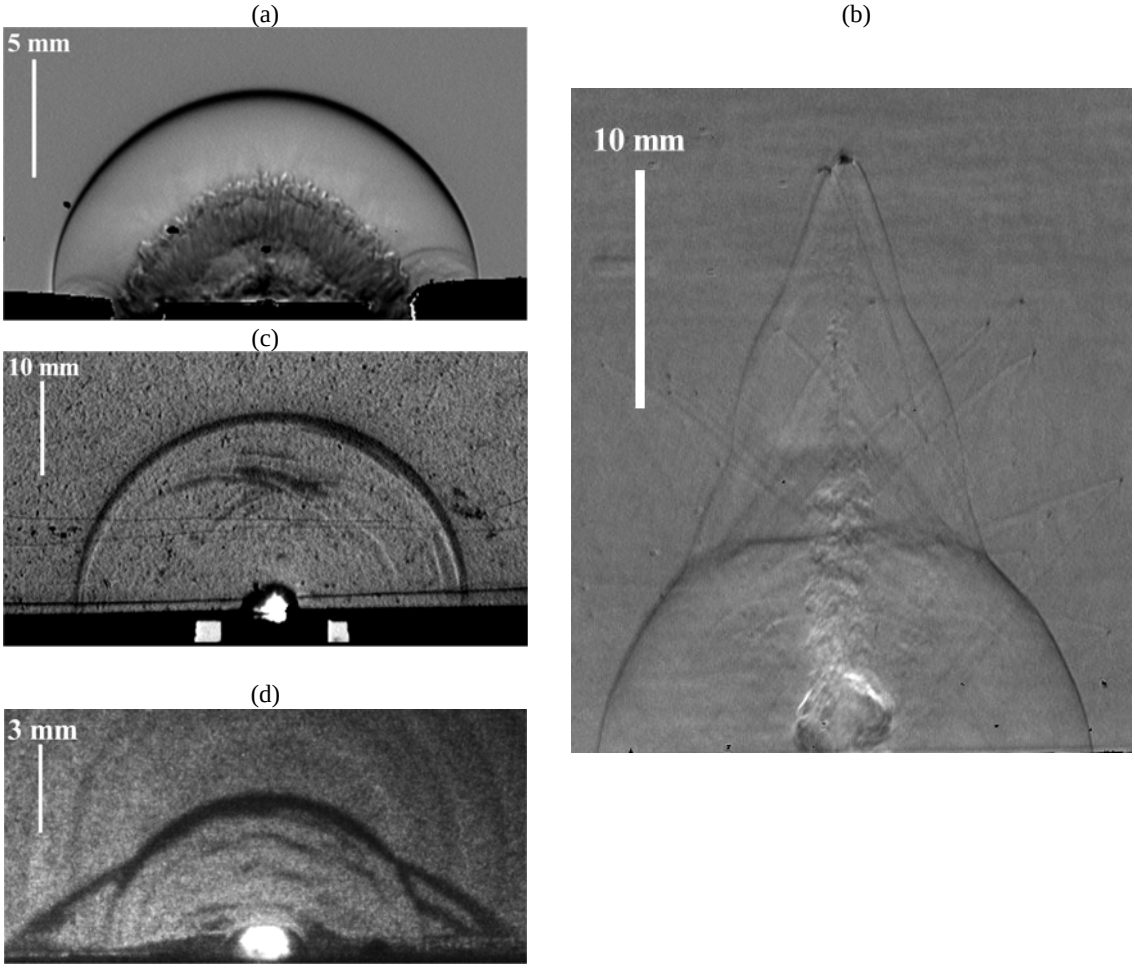


Fig. 5. Representative schlieren images of (a) EBW-induced shock wave in air (b) high-speed flyer plate from slapper detonator (c) EBW-induced shock wave in PDMS (d) and slapper-induced shock wave in PDMS

### 3.2 Velocity vector fields

For both the gas and the polymer trials, standard two-frame cross-correlation analysis is employed utilizing square interrogation spot sizes with 50% spot overlap. The spatial resolution is the extent of the first spot size, which in the case of these experiments is 32 pixels. For the polymer trials, each detonator is placed in intimate contact with the bottom surface of a PDMS witness plate and initiated with an initial charge voltage of 3.02 kV.

Past results for PIV measurements of EBW-induced particle velocities in air are included here for comparisons to be made to results from the witness plate/PIV method. In the gaseous experiments an olive-oil droplet aerosol is used to seed the flow where the droplets have a nominal mean diameter of one micron. Fig. 6 and Fig. 7 display two representative velocity vector fields in air, where the vector spacing is 0.5 mm, and the fields are taken at 17 and 19.5 μs after EBW burst, respectively. These vector fields display the same geometrical trend evident in the schlieren visualization shown in Fig. 5a.

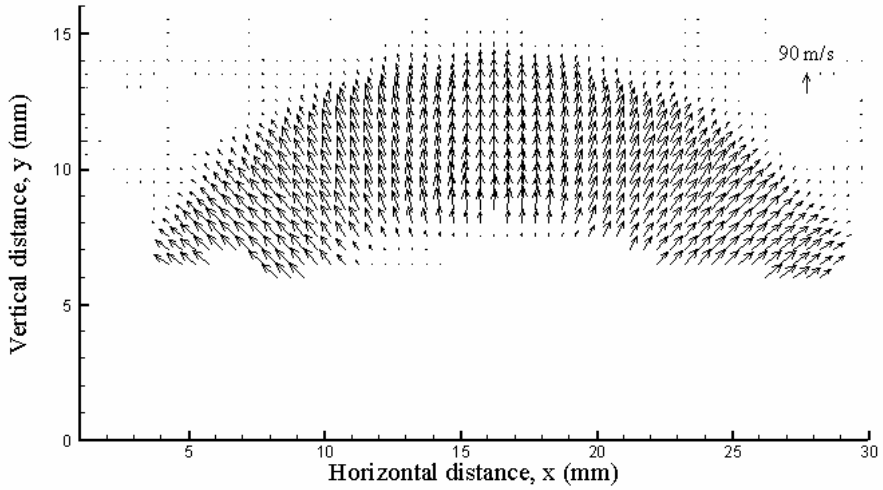


Fig. 6. Field of mean particle-velocity vectors in air measured over the time interval (15, 17) μs with respect to the onset of electrical current through the EBW

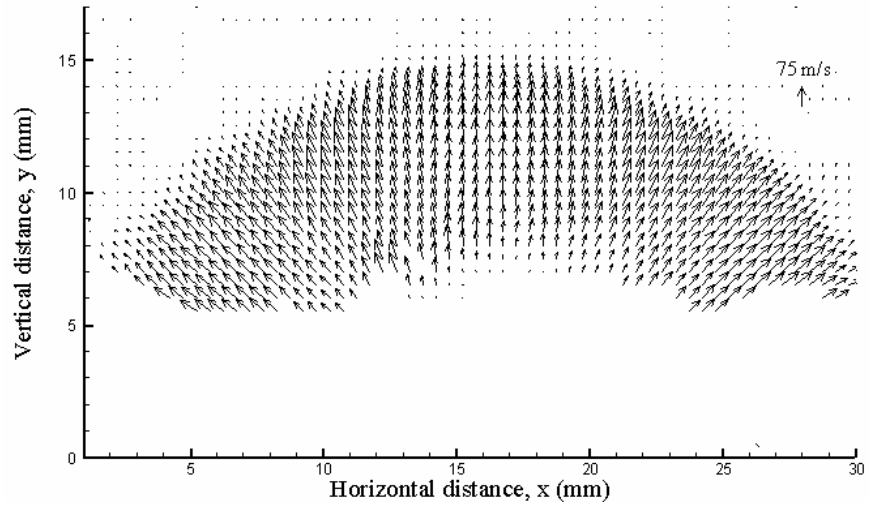


Fig. 7. Field of mean particle-velocity vectors in air measured over the time interval (17.5, 19.5) μs with respect to the onset of electrical current through the EBW

Representative velocity vector fields capturing a plane of EBW and slapper-induced shocks propagating through PDMS witness plates are shown in Fig. 8 and Fig. 9, respectively, where the vector fields are taken at 1.044 μs after EBW burst and 0.954 μs after slapper-bridge burst. Notice

from these vector fields the suggested flow geometry agrees with the schlieren visualizations shown in Fig. 5c and 5d. Also, for nearly equivalent event times of 1.044 μs and 0.954 μs, it is evident that the EBW-induced shock wave is stronger than the slapper-induced shock wave, based on the distance the shock front has traversed in the vertical direction. From inspection of the vector fields, these distances are roughly 2.5 mm and 1.5 mm, respectively.

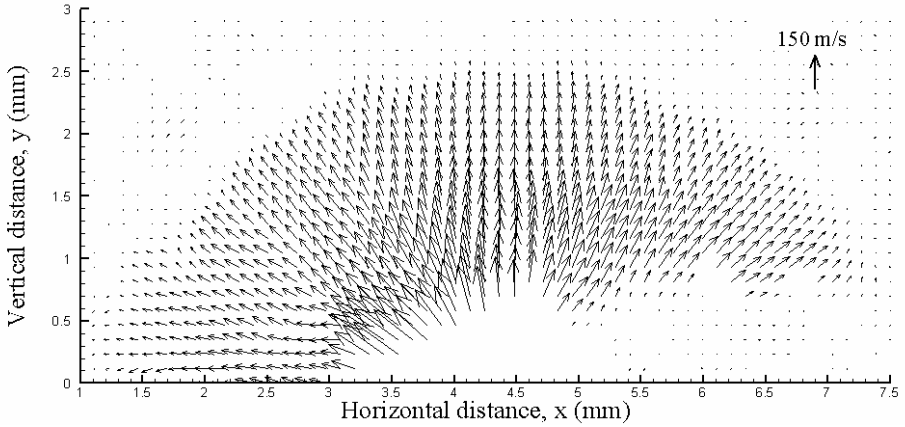


Fig. 8. Field of mean particle-velocity vectors in PDMS measured over the time interval (0.086, 1.13) μs where the burst of the EBW occurred at 0.086 μs

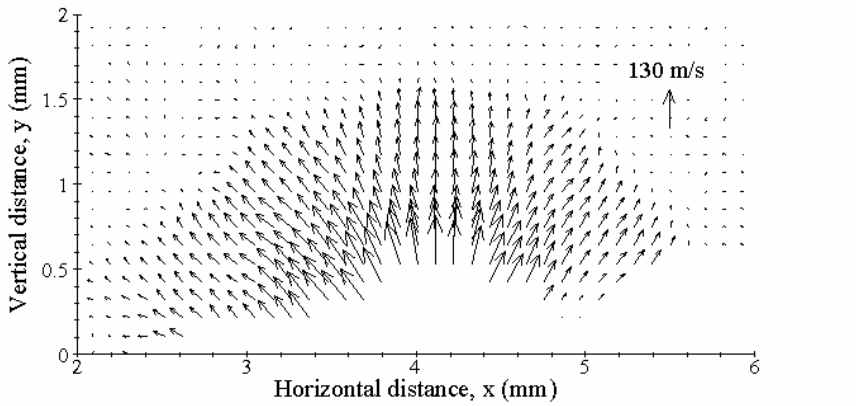


Fig. 9. Field of mean particle-velocity vectors in PDMS measured over the time interval (0.079, 1.033) μs where the burst of the slapper bridge occurred at 0.079 μs

An immediate observation evident by directly comparing the gaseous PIV results with those obtained in PDMS polymers is that the spatial extent of the flow fields is reduced from 15 mm to 1.5 mm. This order of magnitude improvement is accomplished by utilizing the Imacon 200 camera to capture the particle images using 2 μs exposure windows. Such short exposures permit tracer particles to be successfully imaged without incurring effects of pixel saturation due to detonator flash.

The improvement in spatial resolution directly affects the achievable temporal resolution of the PIV system, since the induced shock fronts in PDMS can be investigated for early times after detonator initiation without concern for explosive luminance. This result is evident in the vector field data, where the gaseous flows are investigated at 15 and 17 μs and the flows in the polymers are investigated at just over 1 μs, measured with respect to detonator bridge burst.

### 3.3 Velocity profiles

Due to the suggested curvilinear flow geometry evident in both the schlieren visualizations and the velocity vector field data, plots of speed versus radial distance for multiple polar angles are

made and displayed in Fig. 10. These plots are obtained by interpolating the velocity vector field data along radial lines at polar angles ranging from $\pi/4$ to $3\pi/4$ radians. By observing the plots in Fig. 10a and 10b for the experiments conducted in air, we notice the maximum particle velocity occurs roughly 3 mm behind the location of the shock front. This observation suggests strong particle lag occurs that does not permit the location of the shock front to be determined inside a spatial range of 3 mm.

The speed versus radial distance plots obtained for the PIV trials in PDMS show a large improvement over the gaseous trials with respect to resolving the location of the shock front. Specifically, in the witness plate/PIV method the region of the shock wave is resolved to within the spacing of two velocity vectors. This spacing is the resolution of the velocity vector field data obtained using two-frame cross-correlation analysis with 50% overlap of the interrogation spots. For these experiments the size of the interrogation spot is 32 pixels or 220 μm, on average, giving a mean vector spacing of 110 μm. Hence, the spatial resolution of the velocity field in the region of the shock wave is improved from 3 mm to 220 μm, which is an improvement of a factor of 13. From the plots in Fig. 10c and 10d the location of the shock front is determined to be 1.90 ± 0.11 mm and 1.60 ± 0.11 mm, respectively.

Returning to equation (1) and only considering the quantity $(\rho_p/\rho)^{1/2}$, calculations for olive oil particles in air and metallic-coated glass particles in PDMS can be made. Corresponding values of $(\rho_p/\rho)^{1/2}$ are calculated as 28 for olive oil particles in air at standard conditions and 1.6 for glass particles in PDMS. Based solely on density ratio, equation (1) suggests glass particles in a PDMS medium will be eighteen times more responsive to accelerations than olive oil particles in air. The experimental results appear to confirm the validity of this approximate theoretical prediction.

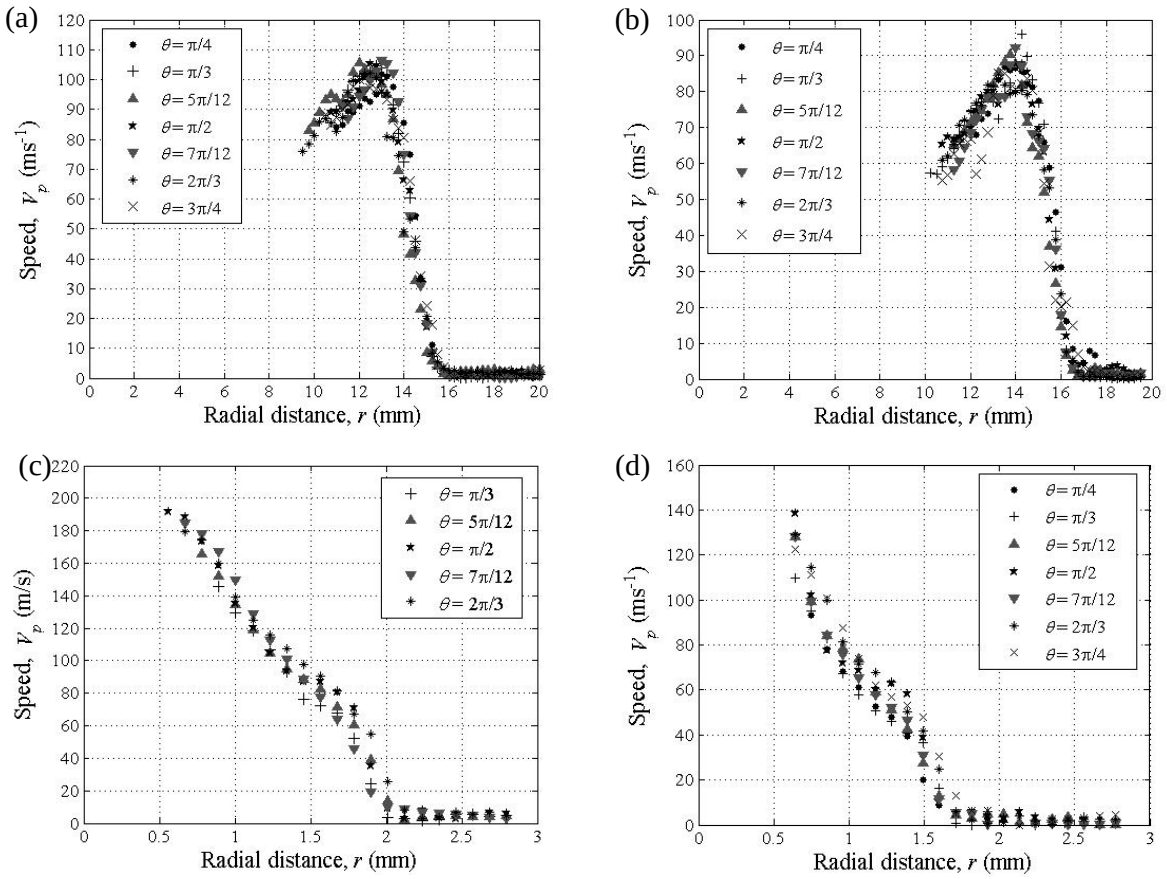


Fig. 10. Speed versus radial distance in (a) air 17 μs after EBW burst (b) air 19.5 μs after EBW burst (c) PDMS 1.044 μs after EBW burst (d) PDMS 0.954 μs after slapper bridge burst

## 4. Summary

The new witness plate/PIV method is successfully shown to be a useful extension of the PIV technique applied to flows containing blast waves from initiation of exploding bridge wire and slapper detonators. The method allows comparative results of effective yield strengths of each detonator to be obtained, and, when coupled with schlieren visualizations, the velocity vector fields provide insight into the induced flow geometries.

Two microsecond exposures from an Imacon 200 high-speed camera are employed to record tracer particle images while attenuating explosive flash inherent in early-time initiation events of EBW and slapper detonators. The short exposure lengths allow an improvement to be made of the resolvable spatial and temporal scales of the flows by at least a factor of ten.

Transitioning from a standard gaseous PIV method using liquid seed particles to a PIV method utilizing solid particles in a polymeric witness plate provides an improvement in particle response of over one order of magnitude. The observed improvement agrees well with an approximate theoretical prediction of the manner in which ratio of seed particle density to fluid density affects particle slip velocity.

Since the resolution of the shock front is limited in these experiments by the size of the measurement tool, i.e. the size of the interrogation spot in correlation analysis, further improvement is still attainable. Larger seed densities of smaller seed particles can be used requiring magnifications larger than unity. This allows the size of the interrogations spots to be reduced. Alternatively, particle-tracking techniques can be used to reduce the limiting size of the interrogation spots. This is done by replacing the average vector from each interrogation spot with the individual velocity vectors comprising each spot. Implementation of this technique will not only increase the number of velocity vectors but will also improve the spatial resolution due to smaller vector-to-vector spacing.

## References

**Adrian R. J.** (1991) Particle-imaging techniques for experimental fluid mechanics. Annual Review of Fluid Mechanics, 23, 261-304

**Balakumar B. J.; Adrian R. J.** (2004) Particle-image velocimetry measurement in the exhaust of a solid rocket motor. Experiments in Fluids, 36, 166-175

**Cartz L. (1995)** *Nondestructive Testing*. Ohio: ASM International

**Cooper P. W.; Kurowski S. R.** (1996) *Introduction to the Technology of Explosives*. New York: Wiley-VCH, Inc.

**Murphy M. J.; Adrian R. J.; Stewart D. S.; Elliott G. S.; Thomas K. A.; Kennedy J. E.** (2005) Visualization of blast waves created by exploding bridge wires. Journal of Visualization, 8, 125-135

**Murphy M. J.; Adrian R. J.** PIV in transparent polymers using a 200 million frame-per-second camera system. 6th International Symposium on Particle Image Velocimetry, Pasadena, California, September 2005